Journal of Industrial and Engineering Chemistry 29 (2015) 120–128

Contents lists available at ScienceDirect

Journal of Industrial and Engineering Chemistry

journal homepage: www.elsevier.com/locate/jiec

# Effect of side chains on solubility and morphology of poly(benzodithiohene-alt-alkylbithiophene) in organic photovoltaics

Min Hee Choi, Kwan Wook Song, Doo Kyung Moon *, Jung Rim Haw *

*Department of Materials Chemistry and Engineering, Konkuk University, 1 Hwayang-dong, Gwangjin-gu, Seoul 143-701, Republic of Korea*

ARTICLE INFO

*Article history:*
Received 16 December 2014
Received in revised form 23 February 2015
Accepted 5 March 2015
Available online 1 April 2015

*Keywords:*
Bithiophene
Benzodithiophene
Side chain
Stille coupling reaction
Bulk heterojunction polymer solar cells

ABSTRACT

It was reported that the side chains play especially an important role in enhancing physical properties and energy levels. Polythiophene based on benzodithiophene has excellent carrier mobility, but high HOMO level. We synthesized polythiophenes, PBDTBiTh(2EH) and PBDTBiTh(12C), were polymerized using the Stille coupling reaction and had thiophene with a 2-ethylhexyl or n-dodecyl side chain. Upon introducing the 2-ethylhexyl side chain, the absorption coefficients of the monomers and polymers were enhanced. Also, the edge-on orientation was fortified and the HOMO level was decreased to −5.37 eV. PBDTBiTh(2EH) showed a power conversion efficiency (PCE) of 2.1%, which was double that of PBDTBiTh(12C).



## Introduction

Organic electronics, polymer light-emitting diodes (PLEDs) [1–5], polymer solar cells (PSCs) [6–10] and polymer field effect transistors (FETs) [11–14] have come into the spotlight because of their light weight, cost-effectiveness and possibility of large-scale production by the solution and roll-to-roll process. Especially, the polymer solar cells, in general, use are of the bulk hetero-junction (BHJ) type, which consist of a p-type semiconductor (conjugated polymer) as the electron donor and n-type semiconductor (fullerene derivatives) as the electron acceptor. The BHJ type of polymer solar cell had the advantages of maximizing the interface between the donor and acceptor and the facile transfer of the charge to the electrode [15]. Over the past decade, polymer solar cells have rapidly developed due to the considerable amount of research that has been done, and power conversion efficiencies (PCEs) of ~8 and ~10% have been reported in a single cell [16] and tandem cell [17], respectively. To commercialize the solar cells and adopt the solution and roll-to-roll process, the solubility and air stability of the polymer at room temperature are very important [18].

Conjugated polymers generally consist of three components, the conjugated backbone, the side chains and the substituents. The conjugated backbone is the major component that determines factors such as the physical properties, energy levels, band gap and inter/intra molecular interactions related to the PSCs [15]. The traditional concept of polymer solar cells was that the bandgap and energy levels were mainly determined by the unit of the conjugated polymer backbone and less-effected by the alkyl solubilizing groups. Therefore, it was considered that the side chains do not affect the short circuit current density ($J_{sc}$) and open circuit voltage ($V_{oc}$) in polymer-based BHJ solar cells. However, in recent studies, it was reported that the alkyl solubilizing groups play a significant role in enhancing the molecular weight, solubility and processability [19]. Additionally, these side chains were found to control the intermolecular interactions and allow for proper mixing with an electron acceptor [15]. Li and Yu reported the synthesis of polymers with different side chains and substituents using thieno[3,4-b]thiophene and benzodithiophene units as the conjugated backbone in 2009 [20]. In spite of having a similar bandgap (~1.60 eV), these polymers showed different highest occupied molecular orbitals (HOMOs), morphologies and PCEs in the range of 2.26–7.4% [20,21]. You *et al.* reported that the energy levels and polymer stacking structure were changed according to the position and length of the side chain [19,22]. In 2013, Beaujuge et al. studied the effect of the number of aliphatic carbons of benzodithiophene and N-alkyl substituted thieno[3,4-c]pyrrole-4,6-dione units and found that the polymer orientation could be engineered and a PCE of 8.5% obtained [23]. Therefore, it is important to choose the length, position and the type of the side chain.

* Corresponding author. Tel.: +82 2 450 3499; fax: +82 2 2201 6447.
*E-mail addresses:* dkmoon@konkuk.ac.kr (D.K. Moon), jrhaw@konkuk.ac.kr (J.R. Haw).

http://dx.doi.org/10.1016/j.jiec.2015.03.024
1226-086X/

Benzodithiophene (BDT) has been widely used in the field of polymer field effect transistors (PFETs) and PSCs, because it has a low intermolecular rotation [24]. As BDT had a rigid and coplanar structure, it shows face-to-face π-stacking, good charge transfer properties and enlarged absorption region, due to its efficient conjugated length. The polythiophenes that were polymerized with BDT and thiophene moieties showed a linear backbone figure of 180°, good charge carrier mobility of 0.01 $cm^2 V^{-1} s^{-2}$ and probability of PFET [25]. The BDT units used did not have any solubilizing groups, but only two *n*-dodecyl alkyl chains introduced into bithiophene. Therefore, the polymers were only soluble in *o*-dichlorobenzene at 100 °C because of their low solubility. Also, a common issue in polymers containing BDT is that they have a high HOMO level and low air stability. The polythiophenes without a side chain showed good hole mobility, but low solubility. For example, poly (3-hexylthiophene) is a famous polymer semiconductor into which the hexyl side chain is introduced, giving it increased solubility. In recent research, it was found that a side chain, of the linear and/or branched type, must be introduced to increase the solubility and processability. Especially, studies involving the introduction of the branched type side chain were recently performed to control the electrical properties of polymer semiconductors [26]. However, according to these side chains, the studies of crystal structure and absorption coefficient of polymer were insufficient.

In this study, polythiophenes containing BDT and bithiophene were polymerized using the Stille coupling condensation. The BDT employed had 2-ethylhexyloxy side chains in the 4 and 8 positions. Also, bithiophene with either 2-ethylhexyl or *n*-dodecyl side chain in the 4 and 4′ positions was used to examine the effect of the type of side chain. The two polythiophenes, PBDTBiTh(2EH) and PBDTBiTh(12C), showed similar polymerized behavior. However, PBDTBiTh(2EH) showed enhanced solubility at room temperature, an edge-on solid phase structure and increased absorption coefficient, but decreased HOMO energy level (−5.37 eV). BHJ PSCs were fabricated using the two polymers mixed with an electron acceptor at room temperature and their increased PCE (2.1%) was confirmed.

## Results and discussion

### *Polymer synthesis*

Scheme 1 reveals the chemical structure of both the monomers and polymers and their synthetic processes. In this study, only p-type π-conjugated polymers were synthesized using 2,6-bis(trimethyltin)-4,8-di-(2-octyldodecyloxy)benzo[1,2-b:4,5-b′]dithiophene (**3**) and two bithiophene derivatives (**4** and **5**). The 2-ethylhexyl and n-dodecyl side chains were introduced into bithiophene derivatives **4** and **5**, respectively. PBDTBiTh(2EH) and PBDTBiTh(12C) were synthesized through the palladium-catalyzed Stille coupling reaction with chlorobenzene as a solvent, $Pd_2dba_3$ and P(o-tolyl)$_3$ as a catalyst and ligand at 90 °C for 48 h. After the polymerization concluded, the polymer was end-capped with bromothiophene and stirred for an additional 12 h. The mixtures were cooled to room temperature, washed with diluted HCl solution, the solvent evaporated and the powder re-precipitated in methanol. The obtained powders were again purified in a Soxhlet apparatus with methanol, acetone and chloroform. Finally, the chloroform-soluble portion was re-precipitated in methanol and a reddish powder obtained. The yields of PBDTBiTh(2EH) and PBDTBiTh(12C) precipitated in methanol were 73 and 98%, respectively. The PBDTBiTh(2EH) was all well soluble in tetrahydrofuran (THF), chlorobenzene and *o*-dichlorobenzene at room temperature, whereas PBDTBiTh(12C) was only soluble at elevated temperature. The structures of the

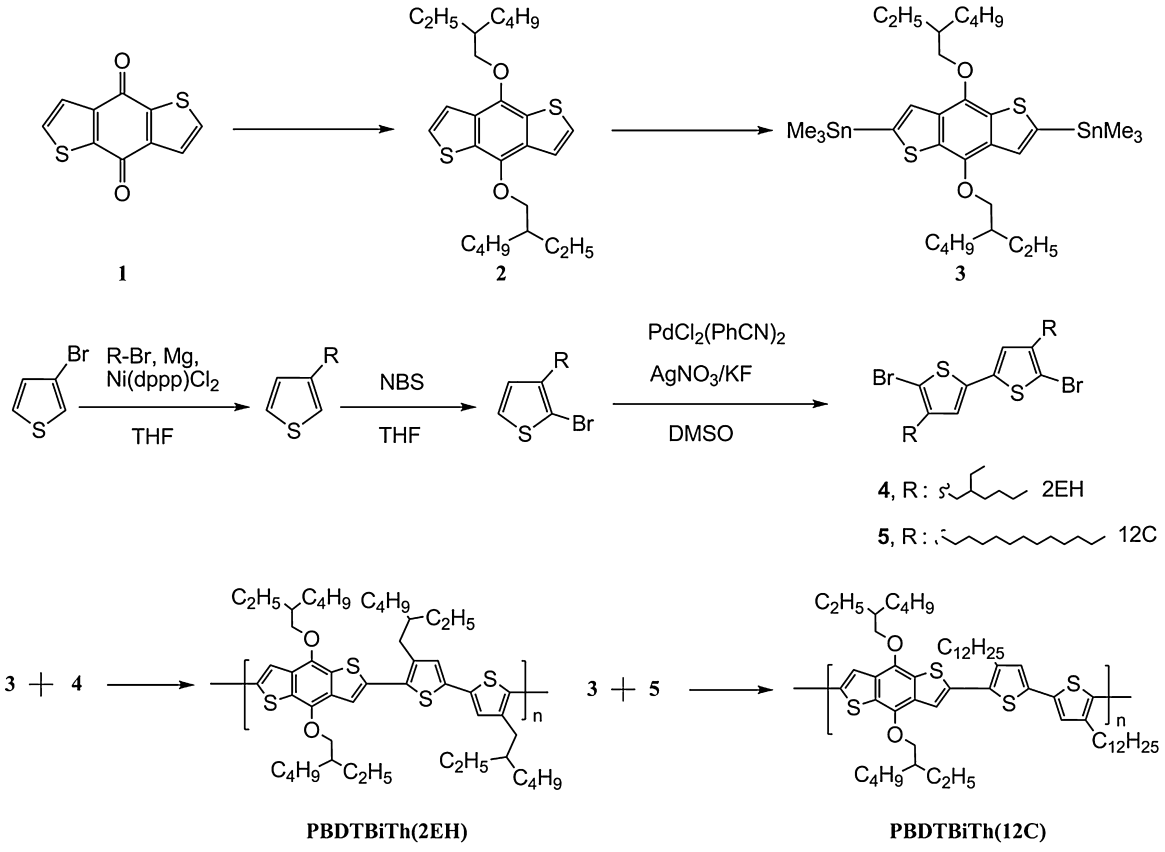


**Scheme 1.** Synthesis of monomers and polymers.

**Table 1**
Molecular weight and thermal property of polymers.

| Polymer | Yield [%] | Mn[a] [kDa] | Mw[a] [kDa] | PDI[a] | Degree of polymerization[b] | $T_d$ (°C)[c] |
|---|---|---|---|---|---|---|
| PBDTBiTh(2EH) | 73 | 29.2 | 53.6 | 1.82 | 33 | 327 |
| PBDTBiTh(12C) | 98 | 25.3 | 54.3 | 2.14 | 26 | 323 |

[a] Determined by GPC in tetrahydrofuran (THF) using polystyrene standards.
[b] Calculated values which Mn is divided by molecular weight of repeating units.[c]Determined by TGA in 5 wt% loss temperature.

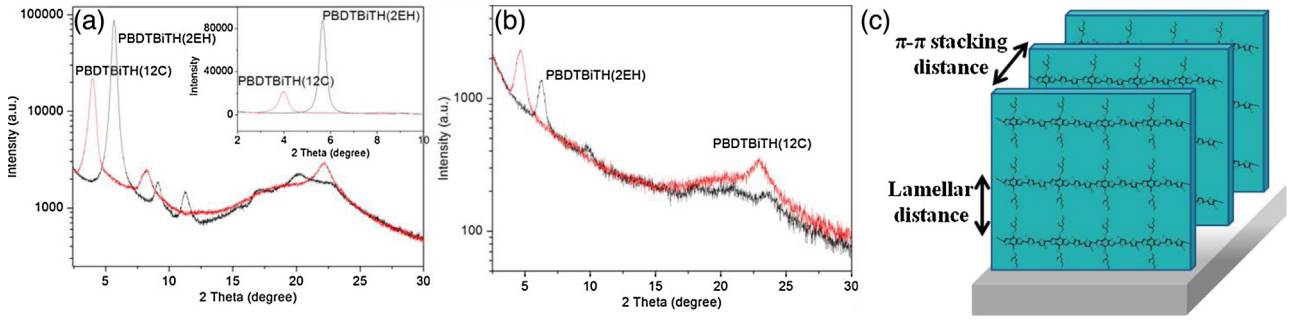


**Fig. 1.** X-ray diffraction patterns of polymers (a) out-of-plane, (b) in-plane and (c) schematic nanomorphology of polymer.

obtained polymers were confirmed with $^1$H NMR spectroscopy (Fig. S1).

Table 1 shows the results of the measurement of the molecular weights of the polymers. PBDTBiTh(2EH) and PBDTBiTh(12C) showed a similar polydispersity index (PDI) (1.82 and 2.14) with number-average molecular weights (Mn) of 29.2 and 25.3 kDa, respectively. However, the degree of polymerization of PBDTBiTh(2EH) was slightly higher than that of PBDTBiTh(12C). Due to the solubility difference of bithiophene derivatives, the solubility of the polymer was affected. Table 1 and Fig. S2 show the results of the thermogravimetric analysis (TGA). PBDTBiTh(2EH) and PBDTBiTh(12C) revealed 5% thermal weight loss at 327 and 323 °C, corresponding to high thermal stability.

*XRD measurements*

Fig. 1 shows the X-ray diffraction measurements of the film to analyze the effects of the side chain of PBDTBiTh(2EH) and PBDTBiTh(12C). The results are summarized in Table 2. Fig. 1(a) shows the diffraction peak in the out-of-plane orientation of the polymers. Both polymers formed an edge-on structure. Also, sharp peaks were observed at 5.64 and 3.97°, which indicated the formation of a highly ordered (1 0 0) lamellar structure. According to the calculation based on Bragg's law ($\lambda = 2d \sin\theta$), the lamellar $d$-spacing distances ($d_1$) were confirmed to be 15.65 and 22.19 Å, respectively, with PBDTBiTh(12C) having a longer $d_1$ than PBDTBiTh(2EH). This is because the distance between polymer chains was determined by the length of the longest chain [19]. Both polymers showed interdigitation and a (2 0 0) peak. The inset of Fig. 1(a) shows the difference in their diffraction intensity. The intensity of the diffraction for PBDTBiTh(2EH) was more than four times that of PBDTBiTh(12C). Therefore, the lamellar structure of the polymer was easily formed by introducing the ethylhexyl chain. In the (0 1 0) crystal plane related to π-π stacking, as shown in Fig. 1(b), diffraction peaks were observed at 20.29 and 22.21° for PBDTBiTh(2EH) and PBDTBiTh(12C), respectively. Also, the calculated π-π stacking distances ($d_\pi$) were 4.37 and 3.87 Å. This is because the p-overlapping distance between the molecules was decreased and a strong intermolecular interaction was formed by the linear dodecyl chain. On the contrary, due to the bulkiness of the branch ethylhexyl chain, the p-overlapping distance between the molecules was increased and the weak intermolecular interaction confirmed [19]. Thus, the two polymers showed an edge-on structure. The lamellar structure formed easily and the lamellar distance was decreased by the ethylhexyl chain. However, the π-overlapping distance and $d_\pi$ were decreased by the dodecyl chain.

**Table 2**
Diffraction angle and d-spacing from XRD spectra.

| Polymer | Plane | polymer only $d$-spacing (Å)/2θ (°) | |
|---|---|---|---|
| | | (100) | (010) |
| PBDTBiTh(2EH) | OOP | 15.65/5.64 | 4.37/20.29 |
| | IP | 13.96/6.32 | 4.37/20.27 |
| PBDTBiTh(12C) | OOP | 22.19/3.97 | 3.99/22.21 |
| | IP | 18.85/4.68 | 3.87/22.89 |

*Optical and electrochemical properties*

Fig. 2 shows the UV–vis spectra of PBDTBiTh(2EH) and PBDTBiTh(12C) in both solution and film. The results are summarized in Table 3. The solution-state spectra were measured at a concentration of 10 μg/ml in chloroform and the film was drop-casted on quartz. The maximum absorption peak ($\lambda_{max}$) of PBDTBiTh(2EH) was 465 nm in solution and its absorption coefficient was calculated to be $7.50 \times 10^4$ M$^{-1}$ cm$^{-1}$. In the case of the PBDTBiTh(2EH) film state, $\lambda_{max}$ was 519 and 561 nm. And, the $\lambda_{max}$ of PBDTBiTh(12C) was 493 nm in solution and its absorption coefficient was calculated to be $5.31 \times 10^4$ M$^{-1}$ cm$^{-1}$. The absorption coefficients of both polymers differed according to the type of introduced side chain.

To calculate the absorption coefficients of the side chains, bithiophene derivatives and polymers, the absorbance was measured according to the concentration, as shown in Fig. 3. In Fig. 3(a)–(e), the UV–visible spectra of 2-ethylhexyl bromide, n-dodecyl bromide and n-octyl bromide to diminish the difference from the number of carbon were showed. According to the Lambert–Beer's law, the absorption coefficient was calculated from the slope of the linear form between absorbance and molarity. The $\lambda_{max}$ values of the three side chains originating from the n–σ* transition were 242 nm and the absorption coefficients of 2-ethylhexyl bromide, n-octyl bromide and n-dodecyl bromide were calculated to be 14.3, 10.5 and 10.1 M$^{-1}$ cm$^{-1}$, respectively.

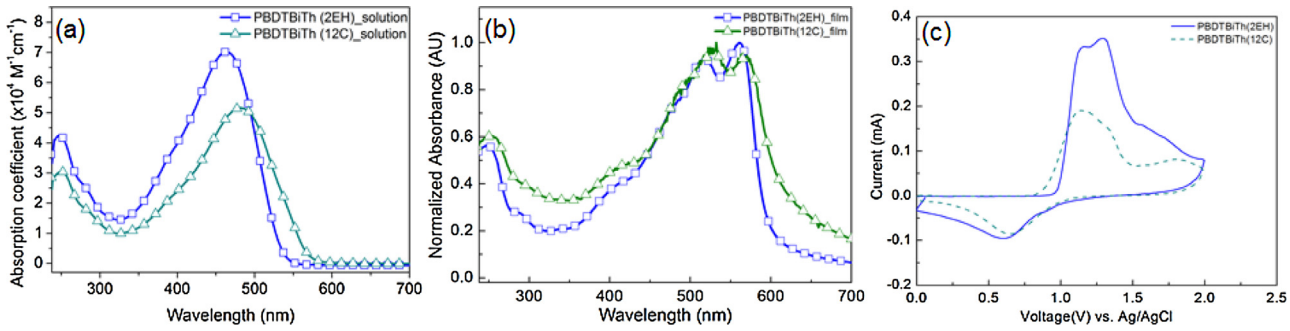


**Fig. 2.** UV–vis spectra of polymers (a) polymers in chloroform solution at concentration of 10 μg/ml (b) polymers in film state and (c) cyclovoltammograms of polymers.

**Table 3**
Optical and electrochemical data of polymers.

| | $CHCl_3$ solution | UV–vis absorption film | | | Cyclic voltammetry | | DFT |
|---|---|---|---|---|---|---|---|
| | $\lambda_{max}$ [nm] | $\lambda_{max}$ [nm] | $\lambda_{onset}$ [nm] | $E_g^{op}$[a] [eV] | $E_{onset,ox}$ (V)/HOMO[eV] | LUMO[b] [eV] | Calcd HOMO [eV] |
| PBDTBiTh(2EH) | 465 | 519, 560 | 605 | 2.05 | 0.99/−5.37 | −3.32 | −5.04 |
| PBDTBiTh(12C) | 493 | 530, 561 | 626 | 1.98 | 0.88/−5.26 | −3.28 | −5.00 |

[a] Calculated from the intersection of the tangent on the low energetic edge of the absorption spectrum with the baseline.
[b] LUMO = HOMO + $E_g^{op}$

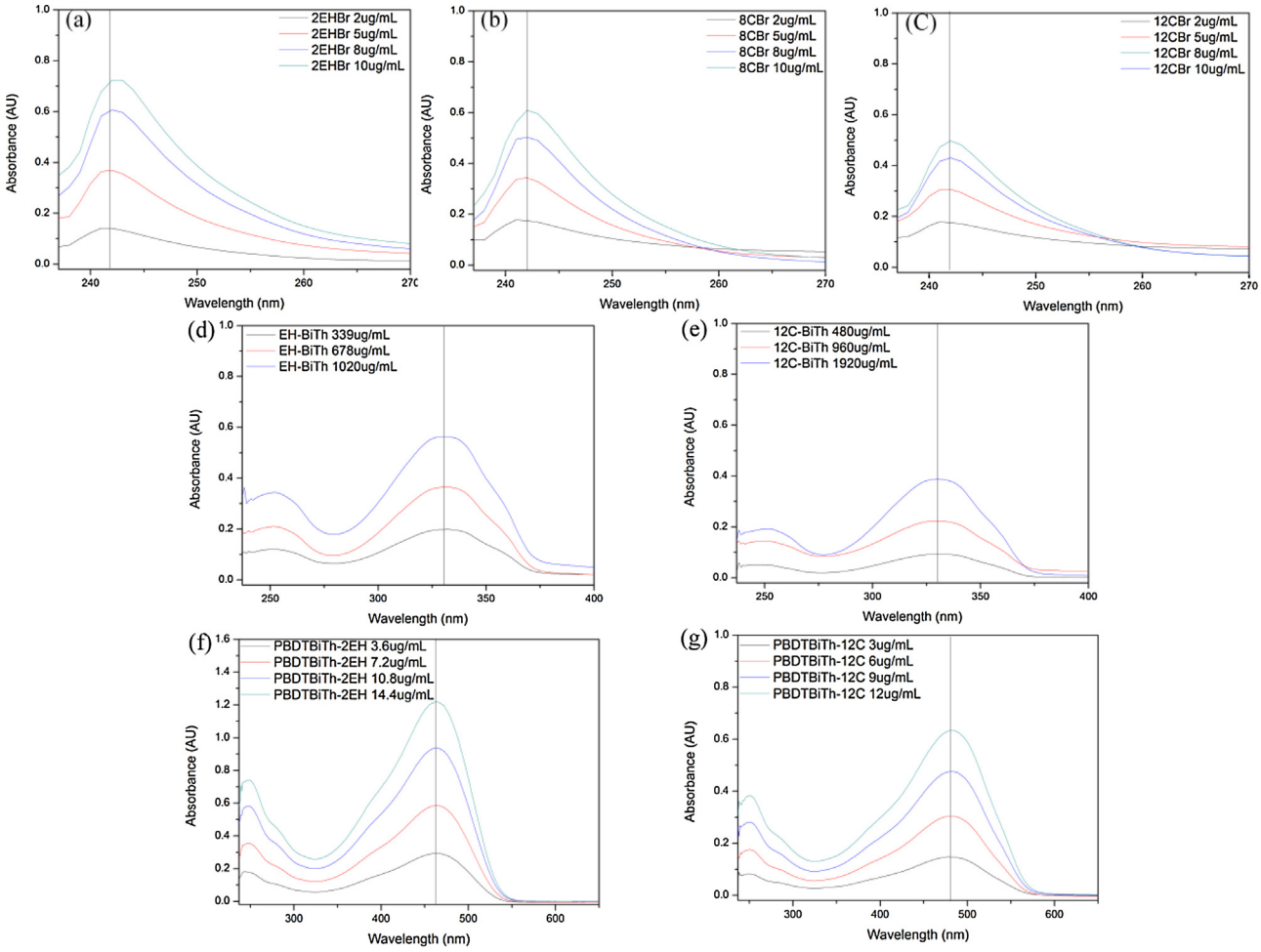


**Fig. 3.** UV–vis spectra of side chains (a–c), bithiophene derivatives (d–e) and polymer (f–g) according to the concentration.

The absorption coefficient was increased by 1.4 times when changing the type of side chain from branched to linear, but did not vary greatly with the number of carbons. Thus, the difference in the absorption coefficients was due to the vibration behavior of the branched chain, which was explained by the Born Oppenheimer approximation and Franck–Condon principle. This is also confirmed for the bithiophene derivatives and their polymers. The $\lambda_{max}$ values of ethylhexyl and dodecyl bithiophene were 330 nm and the absorption coefficients were calculated to be $2.95 \times 10^4$ and $1.31 \times 10^4\ M^{-1}\ cm^{-1}$, respectively, as shown in Fig. 3 (d) and (e). The structure with the branched chain had a bigger absorption coefficient than the linear structure. In the case of the PBDTBiTh(12C) film state, $\lambda_{max}$ was 530 and 561 nm. Compared with the solution state, the UV–visible spectra of PBDTBiTh(2EH) and PBDTBiTh(12C) in the film state were red-shifted by 96 and 37 nm, respectively. This meant that PBDTBiTh(2EH) in the solid state had a more arranged structure and a strong π–π stacking between the polymer molecules [27]. The absorption edges of PBDTBiTh(2EH) and PBDTBiTh(12C) in the film state were 605 and 626 nm and their calculated optical bandgaps ($E_g^{op}$) were 2.05 and 1.98 eV, respectively. Therefore, even though they have the same main chain structure, the $\lambda_{max}$ and absorption range changed according to the type of side chain. Also, the polymer-containing bithiophene with the branched chain had a more arranged structure and a strong π–π stacking between the polymers.

To check the differences in the energy levels as a function of the side chain, the cyclic voltammograms (vs $Fc/Fc^+$) of the PBDTBiTh(2EH) and PBDTBiTh(12C) thin films were measured using 0.1 M tetrabutylammonium-hexafluorophosphate (TBAHFP) in acetonitrile solution, as shown in Fig. 2(c) and summarized in Table 3. The oxidation onset potentials of PBDTBiTh(2EH) and PBDTBiTh(12C) were +0.99 and +0.88 V and their HOMO levels were calculated to be −5.37 and −5.26 eV, respectively. The calculated results indicated that the HOMO energy levels of the polymers tend to increase the side chain length because the introduced longer side chain led to an increase in the electron-donating property of the donor segments. These results are consistent with those reported by Yu's group that the HOMO level of the polymers in the push–pull system is primarily determined by the donor strength [15]. Also Thomson *et al.* reported that the HOMO energy level decreased with increasing ratio of thiophene with ethylhexyl side chain in the main chain due to the effect of the solid-state organization and bulk properties [26]. The polymer was air-stable when the HOMO level of the polymer was lowered below the air oxidation threshold (−5.27 eV vs SCE) [7]. Therefore, PBDTBiTh(2EH) would be expected to be stable when the devices were fabricated. The LUMO energy levels of the polymers were calculated from the difference between the HOMO energy level and the optical band gap. The calculated LUMO energy levels of PBDTBiTh(2EH) and PBDTBiTh(12C) were calculated to be −3.32 and −3.28 eV, respectively. Both polymers had the same main chain structure, but different electrochemical properties according to the type of side chain on the bithiophene moiety. Because of the introduction of the branched ethylhexyl chain, $E_g^{op}$ was slightly increased, but the HOMO and LUMO energy levels were decreased to 0.11 and 0.04 eV, respectively. Accordingly, enhanced $V_{oc}$ and $J_{sc}$ values would be expected when the organic photovoltaics were fabricated.

*Computational study*

Fig. 4 To gain a better understanding of the electronic properties of the synthesized polymers, the molecular geometries and electron densities of the distribution of states were simulated using density functional theory (DFT). The repeating unit was selected as the calculation model. The ethylhexyl and *n*-dodecyl functions of the side chain were simplified to isobutyl and *n*-butyl, respectively. Fig. 4 shows the calculated HOMO, LUMO and dihedral angles for each unit. The HOMO and LUMO orbitals were delocalized to the polymer main chain because, unlike in other low bandgap polymers, there is no electron withdrawing unit. The calculated HOMO levels of PBDTBiTh(2EH) and PBDTBiTh(12C) were −5.04 and −5.00 eV, respectively. As measured in the cyclic voltammograms, the HOMO level of PBDTBiTh(2EH) was lower

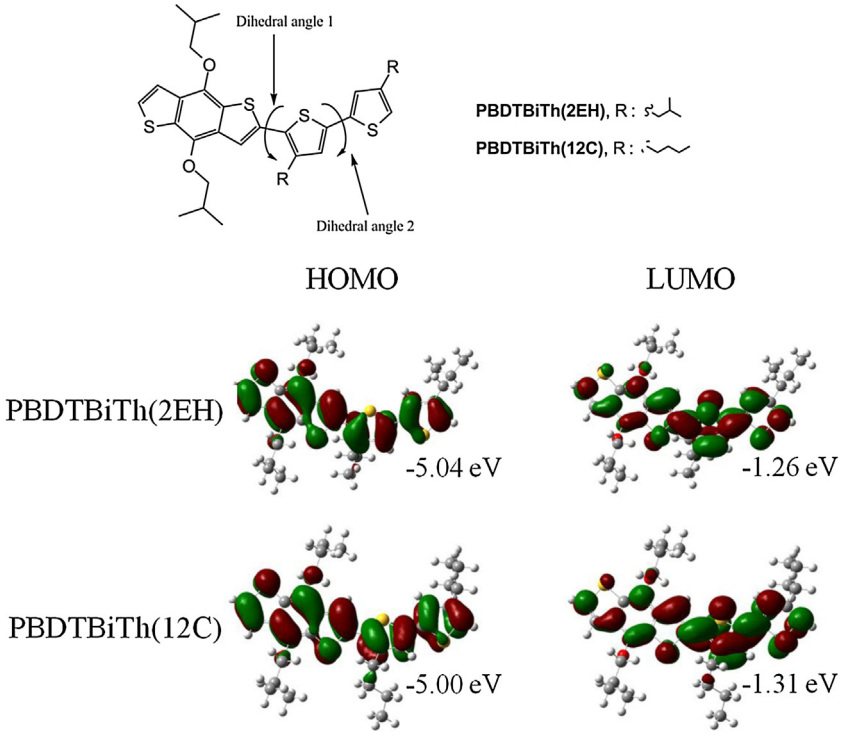


**Fig. 4.** Calculated HOMO, LUMO orbitals and dihedral angles position of polymers.

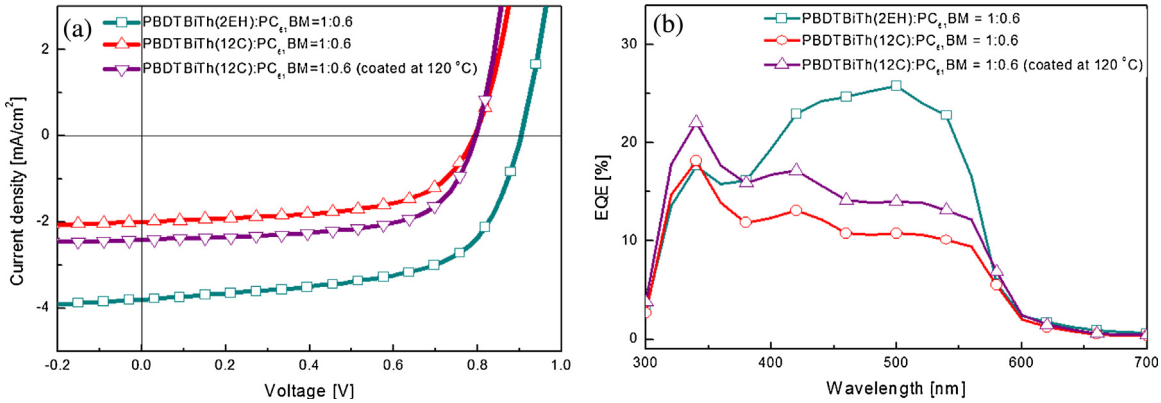


**Fig. 5.** (a) The *J*–*V* curve and (b) the IPCE curve of PBDTBiTh(2EH) and PBDTBiTh(12C).

than that of PBDTBiTh(12C). Thus, the branched side chain decreased the HOMO level of the polymer. In addition, the $\lambda_{max}$ and absorption edge of PBDTBiTh(12C) were red-shifted in the UV−vis spectrum calculated using TD-DFT (Fig. S5). Therefore, the absorption spectrum was blue-shifted by the branched side chain, as measured in the UV−vis spectra.

The dihedral angles were measured between BDT and bithiophene units. The dihedral angles 1 and 2 of PBDTBiTh(2EH) were −142 and 163° and those of PBDTBiTh(12C) were 148 and −161°, respectively. The calculation showed that the type of side chain did not affect the steric hindrance.

*Photovoltaic properties*

Fig. 5 and Table 4 show the photovoltaic (PV) properties of the OPV device consisting of ITO (170 nm)/PEDOT:PSS (40 nm)/active layer (50 nm)/$BaF_2$ (2 nm)/Ba (2 nm)/Al (100 nm). The active layer had an optimized blending ratio obtained by dissolving the polymer and phenyl-C61-butyric acid methyl ester ($PC_{61}BM$) in *o*-dichlorobenzene (*o*-DCB). The open-circuit voltage ($V_{oc}$), short-circuit current ($J_{sc}$), fill factor (FF) and power conversion efficiency (PCE) were 0.899 V, 3.8 mA/cm$^2$, 61.5 and 2.1%, respectively, for PBDTBiTh(2EH), at a ratio of 1:0.6 with $PC_{61}BM$. The PBDTBiTh(2EH) device showed the best performance. PBDTBiTh(2EH) showed not only an enhanced $J_{sc}$ because of its high-ordered edge-on orientation structure, but also increased $V_{oc}$ and FF values due to the lowered HOMO energy level and enhanced solubility afforded by the ethylhexyl side chain. On the contrary, the PCE of PBDTBiTh(12C) is 0.94%. There are three reasons for this; one is the decreased $V_{oc}$ due to the increased HOMO energy level. The difference in the HOMO energy levels of the two polymers was 0.11 eV and that of the $V_{oc}$ values was ~0.1 V. The $V_{oc}$ decreased as the HOMO energy level increased. Another reason is the difference in crystallinity, which is the main factor affecting the charge transfer. Both polymers had an edge-on orientation, but the $J_{sc}$ value of PBDTBiTh(12C) was decreased by its low crystallinity and charge pathway. This result is in good agreement with PBDTBiTh(12C) showed the longer lamellar distance than PBDTBiTh(2EH) at XRD spectra. The last reason is the low solubility because of the strong intermolecular interaction caused by the linear chain [19]. This is a polymer only domain and the generated excitons do not reach the interface of the electron acceptor. As a result, the $J_{sc}$ and FF values are reduced [22]. The $V_{oc}$, $J_{sc}$ and FF values of the PBDTBiTh(12C) device were 0.798 V, 2.0 mA/cm$^2$, 58.9%, respectively. In the case of the polymer with the low solubility, the morphology was improved when it was spin-coated at an elevated temperature. In addition, a pinhole and a particle-free active layer were obtained and the enhancement of the $J_{sc}$, FF and PCE values was confirmed [28]. Therefore, the PBDTBiTh(12C) device was fabricated at 120 °C and the $J_{sc}$ (2.4 mA/cm$^2$), FF (63.4%) and PCE (1.2%) values were improved to 20, 8 and 27%, respectively. In spite of this enhancement, the PCE of PBDTBiTh(2EH) was still relatively high. Therefore, the enhanced solubility and crystallinity due to the ethylhexyl chain were affected by the increase of $J_{sc}$ and PCE. However, the PCE was not increased by the additive. Fig. 5b shows the external quantum efficiency (EQE) of the fabricated devices. As measured in the UV–visible spectra, all of the polymers absorbed light in the range of 300–600 nm. Especially, the EQE in the range of 400–600 nm differed from the behavior of the UV–vis spectra. The absorption coefficient of PBDTBiTh(2EH) was greater than PBDTBiTh(12C), and its EQE was twice as larger of PBDTBiTh(12C), in spite of its large band gap, because PBDTBiTh(2EH) had a high intra-molecular interaction and inter-molecular interaction with PCBM due to its enhanced crystallinity and solubility, respectively.

*Morphology analysis*

Fig. 6 shows the morphology of the polymer/$PC6_1BM$-blend film measured with AFM and TEM. In Fig. 6a, PBDTBiTh(2EH) formed small-size domains that clearly composed the polymer channels. The thin film of PBDTBiTh(2EH) observed smooth film with an 4.7 Å RMS roughness. In contrast, in Fig. 6(d), the polymer channels of PBDTBiTh(12C) could also be observed, but the size of the polymer only domain was ~100 nm due to the interaction between the linear side chains. Accordingly, the RMS roughness of PBDTBiTh(12C) was increased to 9.4 Å. Moulě et al. [29] defined the mixed phase with polymer and PCBM around 0° in the phase image of AFM. Therefore, the mixed phase of PBDTBiTh(2EH) was mostly observed in Fig. 6(b) and (e). Also, the PCBM clusters of PBDTBiTh(2EH) revealed sizes of 10–20 nm and the existence of

**Table 4**
Photovoltaic performances of polymers.

| Polymer | $PC_{61}BM$ ratios | Coated temperature [°C] | $V_{oc}$ [V] | $J_{sc}$ [mA/cm$^2$] | FF [%] | PCE [%] |
|---|---|---|---|---|---|---|
| PBDTBiTh(2EH) | 1:0.6 | 25 | 0.899 | 3.8 | 61.5 | 2.1 |
| PBDTBiTh(12C) | 1:0.6 | 25 | 0.798 | 2.0 | 58.9 | 0.94 |
| | | 120 | 0.798 | 2.4 | 63.4 | 1.2 |

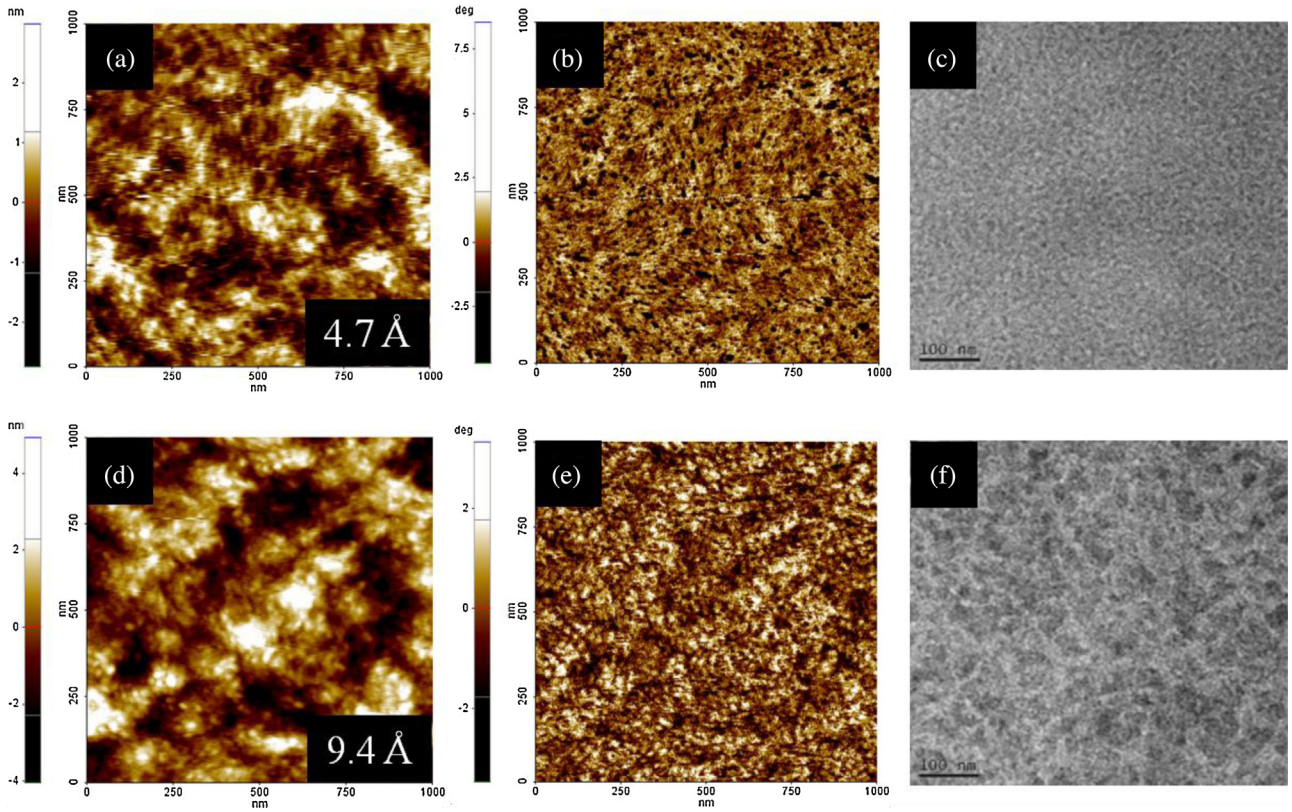


**Fig. 6.** Topographic AFM images (a, d); phase images (b, e); and TEM images (c, f) of PBDTBiTh(2EH):$PC_{61}BM$ (1:0.6, w/w) (a–c) and PBDTBiTh(12C):$PC_{61}BM$ (1:0.6 (w/w)) (d–f).

fine polymer channels was confirmed in Fig. 6(c) and (f). However, the size of the PCBM clusters of PBDTBiTh(12C) was increased to 35–50 nm and the polymer channels were also bigger. Thus, PBDTBiTh(2EH) with the branched chain formed an efficiently mixed phase, because of its favorable mixing with $PC_{61}BM$.

## Conclusions

In this study, two polymers with different side chains were successfully synthesized through the Stille coupling reaction. The polymers consisted of a central BDT core and 2-ethylhexyl or dodecyl thiophene on each side, viz. PBDTBiTh(2EH) and PBDTBiTh(12C), respectively. By introducing the 2-ethylhexyl side chain, the solubility of PBDTBiTh(2EH) at room temperature and absorption coefficient were enhanced due to the difference in their molecular vibration energy. According to the XRD measurement, the formation of a polymer lamellar structure was facilitated by the branched chain. Also, even though the polymer backbone was the same, the HOMO energy level of the polymer with the branched side chain was decreased below the air oxidation threshold due to the solid-state organization effect. There was no effect on the dihedral angle, but the crystallinity and intra-molecular interaction were enhanced according to the type of side chain. Finally, as a result of the favorable mixing with PCBM, the $J_{sc}$ and PCE values were increased by two-fold. In conclusion, the performance of polymer electronics can be improved by controlling the position and type of side chain.

## Experimental

### *Materials*

All starting materials were purchased from Sigma Aldrich and Alfar Aesar, and used without further purification. Toluene and tetrahydrofuran (THF) were distilled from benzophenone ketyl and sodium. 3-dodecylthiophene [30], 2,6-bis(trimethyltin)-4,8-bis(2-ethylhexyloxy)benzo[1,2-b:4,5-b′]-dithiophene (**3**) [20] were prepared according to the methods reported in the literature.

**3-(2-Ethylhexyl)thiophene**

The Grignard reagent was prepared from 2-ethylhexyl bromide (10 g, 40.4 mmol), and magnesium turnings (1.015 g, 41.78 mmol) in THF (14 ml) and refluxed for 1 h. It was slowly added to a mixture of 3-bromothiophene (5.046 g, 31 mmol) and Ni(dppp)$Cl_2$ (0.1677 g, 0.309 mmol) in 10 ml of THF at 0 °C. The mixture was warmed to room temperature for 24 h before being quenched by diluted HCl. The aqueous layer was extracted with ether and combined with all the organic layers. The solvent was evaporated after drying over $MgSO_4$. The product was purified by vacuum distillation. Yield: 4.37 g (72%). $^1$H NMR (400 MHz; $CDCl_3$ $Me_4Si$, d, ppm): 7.22–7.21 (m, 1H; Ar), 6.9–6.89 (m, 2H; Ar,) 2.56 (d, 2H; $CH_2$), 1.56–1.55 (m, 1H; CH), 1.32–1.19 (m, 8H; $CH_2$), 0.91–0.82 (m, 6H; $CH_3$).

**2-Bromo-3-(2-ethylhexyl)thiophene**

Into a stirred solution of 3-(2-ethylhexyl)thiophene (3.2 g, 16.297 mmol) in $CHCl_3$-acetic acid (1:1 (v/v) 32.6 ml) was portion wise added NBS (2.9 g, 16.3 mmol), and the mixture was stirred at RT for 24 h. The mixture was poured into water and extracted with chloroform. The extract was successively washed with aqueous $NaHCO_3$ solution and dried with $Na_2SO_4$. The solvent was evaporated and the residue was purified by column chromatography on silica gel with hexane and short path distillation, respectively. Yield 2.94 g (60%). $^1$H NMR (400 MHz; $CDCl_3$ $Me_4Si$, d, ppm): 7.18–7.17 (d, 1H; Ar), 6.77–6.75 (d, 2H; Ar), 2.50–2.48 (d, 2H; $CH_2$), 1.62–1.56 (m, 1H; CH), 1.33–1.18 (m, 8H; $CH_2$), 0.91–0.81 (m, 6H; $CH_3$).

**5,5′-Dibromo-4,4′-bis(2-ethylhexyl)-2,2′-bithiophene (4)**

2-Bromo-3-(2-ethylhexyl)thiophene (1.47 g, 5.354 mmol) was weighed into a flask. Anhydrous dimethylsulfoxide (DMSO) (24 ml) was added to the flask and the mixture was heated to

70 °C. Silver nitrate (1.82 g, 10.71 mmol), potassium fluoride (0.622 g, 10.71 mmol) and bis(benzonitrile)palladium (II) chloride (41 mg, 2 mol.%) were added in one portion, and the resulting mixture was stirred at 70 °C. Two additional portions of $AgNO_3$ and KF (same quantities as above) were added after 3 and 6 h and the mixture was stirred overnight at the same temperature. The mixture was then cooled, filtered through a short silica column, and washed three times with water. The title compound (2.42 g, 54%) was obtained as yellow oil after column chromatography on silica with hexane as the eluent. Yield 1.13 g (77.0%). $^1$H NMR (400 MHz, $CDCl_3$, $\delta$, ppm): 6.74 (s, 2H; Ar), 2.46–2.44 (d, 4H; $CH_2$), 1.61–1.55 (m, 2H; CH), 1.33–1.28 (m, 16H; $CH_2$), 0.91–0.87 (m, 12H; $CH_3$).

**2-Bromo-3-dodecylthiophene**

The preparation of 2-bromo-3-dodecylthiophene was carried out as described for 2-bromo-3-(2-ethylhexyl)thiophene. In this case, 3-(2-dodecyl)thiophene (2.01 g, 7.969 mmol), NBS (1.418 g, 7.969 mmol) and THF (19.92 ml) were used. Yield 3.247 g (56.0%). $^1$H NMR (400 MHz; $CDCl_3$ $Me_4Si$, $\delta$, ppm): 7.25–7.17 (d, 1H; Ar), 6.79–6.78 (d, 2H; Ar,), 2.57–2.53 (t, 2H; $CH_2$), 1.30–1.25 (m, 20H; $CH_2$), 0.90–0.86 (t, 3H; $CH_3$).

**5,5′-Dibromo-4,4′-didodecyl-2,2′-bithiophene (5)**

The preparation of 5,5′-dibromo-4,4′-didodecyl-2,2′-bithiophene (**5**) was carried out as described for 5,5′-dibromo-4,4′-bis(2-ethylhexyl)-2,2′-bithiophene (**4**). In this case, 2-bromo-3-dodecylthiophene (1.61 g, 4.861 mmol), potassium fluoride (0.564 g, 9.722 mmol), silver nitrate (1.651 g, 9.722 mmol), bis(-benzonitrile)palladium(II)chloride (0.018 g, 0.048 mmol) and anhydrous DMSO (24.3 ml) were used. Yield 0.415 g (13.0%). $^1$H NMR (400 MHz, $CDCl_3$, d, ppm): 6.79–6.77 (s, 2H; Ar), 2.53–2.49 (t, 4H; CH2), 1.31–1.26 (m, 40H; CH2), 0.88–0.86 (t, 6H; $CH_3$).

*Polymerization through the Stille coupling reaction*

**Poly[(4,8-di-(2-ethylhexyloxy)benzo[1,2-b:4,5-b′]dithiophene-2,6-diyl)-alt-(5,5′-yl-4,4′-bis(2-ethylhexyl)-2,2′-bithiophene)] [PBDTBiTh(2EH)]**

2,6-Bis(trimethyltin)-4,8-bis(2-ethylhexyloxy)benzo[1,2-b:4,5-b′]-dithiophene (**3**) (0.2316 g, 0.3 mmol), 5,5′-dibromo-4,4′-bis(2-ethylhexyl)-2,2′-bithiophene (**4**) (0.1645 g, 0.3 mmol), $Pd_2dba_3(0)$ (0.01 g, 0.012 mmol), and P(o-tolyl)$_3$ (0.0146 g, 0.048 mmol) were dissolved in chlorobenzene (10 ml). The flask was degassed and refilled with nitrogen gas twice. The polymerization mixture was stirred at 90 °C for 48 h, and a few drops of 2-bromothiophene were added. After 12 h, a few drops of 2-tributylstannyl thiophene were also added for the end-capping reaction. The reaction mixture was cooled to room temperature and poured into methanol. The precipitate was filtered and purified with methanol, acetone, hexane and chloroform in a Soxhlet apparatus. The polymer was precipitated in methanol. Finally, the polymer was collected as a reddish solid. Yield 0.1889 g (73.0%). $^1$H NMR (400 MHz, $CDCl_3$, d, ppm): 8.19–8.10(m), 7.82–7.69(m), 7.57–7.38(m), 4.17(br, 4H), 1.90(br, 4H), 1.53–1.23(m), 0.90–0.64(m). Anal. calcd. for $C_{50}H_{74}O_2S_4$: C 71.89, H 8.93, O 3.83, S 15.35; found: C 71.21, H 8.61, O 3.81, S 15.03.

**Poly[(4,8-di-(2-ethylhexyloxy)benzo[1,2-b:4,5-b′]dithiophene-2,6-diyl)-alt-(5,5′-yl-4,4′-bis(dodecyl)-2,2′-bithiophene)] [PBDTBiTh(12C)]**

2,6-Bis(trimethyltin)-4,8-bis(2-ethylhexyloxy)benzo[1,2-b:4,5-b′]-dithiophene (**3**) (0.2316 g, 0.3 mmol), 5,5′-dibromo-4,4′-didodecyl-2,2′-bithiophene (**5**) (0.1645 g, 0.3 mmol), $Pd_2dba_3(0)$ (0.01 g, 0.012 mmol), and P(o-tolyl)$_3$ (0.0146 g, 0.048 mmol) were dissolved in chlorobenzene (10 ml). The flask was degassed and refilled with nitrogen gas twice. The polymerization mixture was stirred at 90 °C for 48 h, and a few drops of 2-bromothiophene were added. After 12 h, a few drops of 2-tributylstannyl thiophene were also added for the end-capping reaction. The reaction mixture was cooled to room temperature and poured into methanol. The precipitate was filtered and purified with methanol, acetone, hexane and chloroform in a Soxhlet apparatus. The polymer was precipitated in methanol. Finally, the polymer was collected as a reddish solid. Yield 0.253 g (98.0%). $^1$H NMR (400 MHz, $CDCl_3$, d, ppm): 8.19–8.10(m), 7.82–7.69(m), 7.57–7.38(m), 4.17(br, 4H), 1.90(br, 4H), 1.53–1.23(m), 0.90–0.64(m). Anal. calcd. for $C_{58}H_{90}O_2S_4$: C 73.51, H 9.57, O 3.38, S 13.54; found: C 71.81, H 8.86, O 3.93, S 14.51.

*Measurements*

The $^1$H MR (400 MHz) spectra were recorded using a Brüker AMX400 spectrometer in $CDCl_3$, and the chemical shifts were recorded in units of ppm with TMS as the internal standard. The absorption spectra were recorded using an Agilent 8453 UV–vis spectroscopy system. The solutions that were used for the UV–vis spectroscopy measurements were dissolved in chloroform at a concentration of 10 μg/ml. The films were drop-coated from the chloroform solution onto a quartz substrate. All of the GPC analyses were carried out using THF as the eluent and a polystyrene standard as the reference. The TGA measurements were performed using a TG 209 F3 thermogravimetric analyzer. The cyclic voltammetric waves were produced using a Zahner IM6eX electrochemical workstation with a 0.1 M acetonitrile (substituted with nitrogen for 20 min) solution containing tetrabutylammonium hexafluorophosphate ($Bu_4NPF_6$) as the electrolyte at a constant scan rate of 50 mV/s. ITO, a Pt wire, and silver/silver chloride [Ag in 0.1 M KCl] were used as the working, counter and reference electrodes, respectively. The electrochemical potential was calibrated against $Fc/Fc^+$. The HOMO levels of the polymers were determined using the oxidation onset value. Onset potentials are values obtained from the intersection of the two tangents drawn at the rising current and the baseline changing current of the CV curves. The LUMO levels were calculated from the differences between the HOMO energy levels and the optical band-gaps, which were determined using the UV–vis absorption onset values in the films. The current density–voltage ($J$–$V$) curves of the photovoltaic devices were measured using a computer-controlled Keithley 2400 source measurement unit (SMU) that was equipped with a Class A Oriel solar simulator under an illumination of AM 1.5G (100 mW/cm$^2$). Topographic images of the active layers were obtained through atomic force microscopy (AFM) in tapping mode under ambient conditions using an XE-100 instrument.

*Photovoltaic cell fabrication and treatment*

All the bulk-heterojunction PV cells were prepared using the following device fabrication procedure. The glass/indium tin oxide (ITO) substrates [Sanyo, Japan 10 Ω/γ)] were sequentially patterned lithographically, cleaned with detergent, ultrasonicated in deionized water, acetone and isopropyl alcohol, dried on a hot plate at 120 °C for 10 min, and treated with oxygen plasma for 10 min to improve the contact angle just before film coating. Poly(3,4-ethylene-dioxythiophene):poly(styrene-sulfonate) (PEDOT:PSS, Baytron P 4083 Bayer AG) was passed through a 0.45 mm filter before being deposited on ITO at a thickness of ca. 32 nm by spin-coating at 4000 rpm in air, and then dried at 120 °C for 20 min inside a glove box. A blend of 1-(3-methoxycarbonyl)propyl-1-phenyl-[6,6]-C71 (PC71BM) and the polymer [1:2 (w/w), 1:4 (w/w)] at a concentration of 7.5 mg ml$^{-1}$ in chlorobenzene was stirred overnight, filtered through a 0.2 mm poly(tetrafluoroethylene) (PTFE) filter, and then spin-coated (500–3000 rpm, 30 s) on top of the PEDOT:PSS layer. The device was completed by depositing thin layers of $BaF_2$ (1 nm) and Ba (2 nm) as an electron injection cathode, followed by the deposition of a 200 nm thick aluminum

layer at pressures less than $10^{-6}$ Torr. The active area of the device was 4 $mm^2$. Finally, the cell was encapsulated using UV-curing glue (Nagase, Japan).

## Conflict of interest

The authors declare no competing financial interest.

## Acknowledgments

This paper was written as part of Konkuk University's research support program for its faculty on sabbatical leave in 2013.

## Appendix A. Supplementary data

Supplementary data associated with this article can be found, in the online version, at doi:10.1016/j.jiec.2015.03.024.

## References

[1] R.H. Friend, R.W. Gymer, A.B. Holmes, J.H. Burroughes, R.N. Marks, C. Taliani, D.D.C. Bradley, D.A.D. Santos, J.L. Bredas, M. Logdlund, W.R. Salaneck, Nature 397 (1999) 121–128.
[2] G. Gustafsson, Y. Cao, G.M. Treacy, F. Klavetter, N. Colaneri, A.J. Heeger, Nature 357 (1992) 477–479.
[3] M.M. Alam, S.A. Jenekhe, Chem. Mater. 14 (2002) 4775–4780.
[4] W. Lu, J. Kuwabara, T. Kanbara, Macromolecules 44 (2011) 1252–1255.
[5] H.J. Song, J.Y. Lee, I.S. Song, D.K. Moon, J.R. Haw, J. Ind. Eng. Chem. 17 (2011) 352–357.
[6] J.-Y. Lee, W.-S. Shin, J.-R. Haw, D.-K. Moon, J. Mater. Chem. 19 (2009) 4938–4945.
[7] J.-Y. Lee, S.-H. Kim, I.-S. Song, D.-K. Moon, J. Mater. Chem. 21 (2011) 16480–16487.
[8] F.C. Krebs, Sol. Energy Mater. Sol. C 93 (2009) 465–475.
[9] C.S. Tao, J. Jiang, M. Tao, Sol. Energy Mater. Sol. C. 95 (2011) 3176–3180.
[10] J. Kuwabara, Y. Nohara, S.J. Choi, Y. Fujinami, W. Lu, K. Yoshimura, J. Oguma, K. Suenobu, T. Kanbara, Polym. Chem. 4 (2013) 947–953.
[11] B.-L. Lee, T. Yamamoto, Macromolecules 32 (1999) 1375–1382.
[12] I. McCulloch, M. Heeney, C. Bailey, K. Genevicius, I. MacDonald, M. Shkunov, D. Sparrowe, S. Tierney, R. Wagner, W. Zhang, M.L. Chabinyc, R.J. Kline, M.D. McGehee, M.F. Toney, Nat. Mater. 5 (2006) 328–333.
[13] T. Yamamoto, H. Kokubo, M. Kobashi, Y. Sakai, Chem. Mater. 16 (2004) 4616–4618.
[14] T. Yasuda, Y. Sakai, S. Aramaki, T. Yamamoto, Chem. Mater. 17 (2005) 6060–6068.
[15] H. Zhou, L. Yang, W. You, Macromolecules 45 (2012) 607–632.
[16] M. Zhang, Y. Gu, X. Guo, F. Liu, S. Zhang, L. Huo, T.P. Russell, J. Hou, Adv. Mater. (2013).
[17] J. You, L. Dou, K. Yoshimura, T. Kato, K. Ohya, T. Moriarty, K. Emery, C.-C. Chen, J. Gao, G. Li, Y. Yang, Nat. Commun. 4 (2013) 1446.
[18] K. Norrman, M.V. Madsen, S.A. Gevorgyan, F.C. Krebs, J. Am. Chem. Soc. 132 (2010) 16883–16892.
[19] L. Yang, H. Zhou, W. You, J. Phys. Chem. C 114 (2010) 16793–16800.
[20] Y. Liang, D. Feng, Y. Wu, S.-T. Tsai, G. Li, C. Ray, L. Yu, J. Am. Chem. Soc. 131 (2009) 7792–7799.
[21] Y. Liang, Z. Xu, J. Xia, S.-T. Tsai, Y. Wu, G. Li, C. Ray, L. Yu, Adv. Mater. 22 (2010) E135–E138.
[22] H. Zhou, L. Yang, S. Xiao, S. Liu, W. You, Macromolecules 43 (2010) 811–820.
[23] C. Cabanetos, A. El Labban, J.A. Bartelt, J.D. Douglas, W.R. Mateker, J.M.J. Fréchet, M.D. McGehee, P.M. Beaujuge, J. Am. Chem. Soc. 135 (2013) 4656–4659.
[24] L. Huo, J. Hou, Polym. Chem. 2 (2011) 2453.
[25] R. Rieger, D. Beckmann, A. Mavrinskiy, M. Kastler, K. Müllen, Chem. Mater. 22 (2010) 5314–5318.
[26] B. Burkhart, P.P. Khlyabich, B.C. Thompson, Macromolecules 45 (2012) 3740–3748.
[27] K. Yao, L. Chen, T. Hu, Y. Chen, Org. Elec. 13 (2012) 1443–1455.
[28] J. Liu, H. Choi, J.Y. Kim, C. Bailey, M. Durstock, L. Dai, Adv. Mater. 24 (2012) 538–542.
[29] A.J. Moulé, A. Tsami, T.W. Bünnagel, M. Forster, N.M. Kronenberg, M. Scharber, M. Koppe, M. Morana, C.J. Brabec, K. Meerholz, U. Scherf, Chem. Mater. 20 (2008) 4045–4050.
[30] Y. Li, T.-H. Kim, Q. Zhao, E.-K. Kim, S.-H. Han, Y.-H. Kim, J. Jang, S.-K. Kwon, J. Polym. Sci. Part A: Polym. Chem. 46 (2008) 5115–5122.